Biophysical Journal
Article

Biophysical Society

Investigation of the Melting Behavior of DNA Three-Way Junctions in the Closed and Open States

Carolyn E. Carr[1] and Luis A. Marky[1,*]
[1]Department of Pharmaceutical Sciences, University of Nebraska Medical Center, Nebraska Medical Center, Omaha, Nebraska

ABSTRACT Intramolecular three-way junctions are commonly found in both DNA and RNA. These structures are functionally relevant in ribozymes, riboswitches, rRNA, and during replication. In this work, we present a thermodynamic description of the unfolding of DNA intramolecular three-way junctions. We used a combination of spectroscopic and calorimetric techniques to investigate the folding/unfolding thermodynamics of two three-way junctions with a closed (*Closed-J*) or open (*Open-J*) junction and their appropriate control stem-loop motifs (*GAAATT-Hp*, *CTATC-Hp*, and *Dumbbell*). The overall results show that both junctions are stable over a wide range of salt concentrations. However, *Open-J* is more stable due to a higher enthalpy contribution from the formation of a higher number of basepair stacks whereas *Closed-J* has a defined structure and retains the basepair stacking of all three stems. The comparison of the experimental results of *Closed-J* and *Open-J* with those of their component stem-loop motifs allowed us to be more specific about their cooperative unfolding. For instance, *Closed-J* sacrifices thermal stability of the *Dumbbell* structure to maintain an overall folded state. At higher salt concentration, the simultaneous unfolding of the above domains is lost, resulting in the unfolding of the three separate stems. In contrast, the junction of *Open-J* in low salt retains the thermal and enthalpic stability of the *Dumbbell* structure although sacrificing stability of the CTATC stem. The relative stability of *Dumbbell* is the primary reason for the higher $\Delta G^{\circ}_{(5)}$, or free energy, value seen for *Open-J* at low salt. Higher salt not only maintains thermal stability of the *Dumbbell* structure in *Open-J* but causes the CTATC stem to fully fold.

INTRODUCTION

Single-stranded DNA with a sequence that is partially complementary to itself can form an intramolecular structure. The structure that is formed can be precisely predicted if the sequence is known. Both DNA and RNA are known to form complex and varied secondary structures involved in gene regulation. To understand how these structures fold, and thus to understand how these structures control gene regulation, a complete physical description is needed. The physical parameters that dictate folding are dependent on the basepairing, base-stacking, hydration, and ion binding of the folded oligonucleotide structures.

Intramolecular junctions are commonly found in both DNA and RNA molecules and have important functional roles (1,2). Closed three-way intramolecular junctions are commonly found in naked RNA and mRNA structures such as riboswitches (1,3,4) and ribozymes (1,5–7), as well as ribonucleoprotein structures such as rRNA (8,9) and the signal recognition particle (10–13). These regulatory elements control gene expression, protein synthesis, and protein localization within the cell. Closed three-way junctions are also found in DNA during replication (14–16) and recombination (2,17–20). A closed junction is one in which the 5′ and 3′ ends of the oligonucleotide meet at the end of one of the stems, which leads to a tight intramolecular junction that is not influenced by fraying caused by an open stem. The structure of *Closed-J* in Fig. 1 is an example of a closed three-way junction. The replication fork that forms during transcription or rolling circle-replication is an example of an open three-way junction in DNA (21,22). An open junction is one in which the three stems meet at the junction but in which the 5′ and 3′ ends are not linked by a phosphodiester bond and so the junction is open; the structure of *Open-J* (Fig. 1) is an example of an open three-way junction. Three-way junctions are involved in various important biological functions (1,2,15,21) and it is therefore of considerable interest to determine the structure and physical properties that dictate folding and unfolding of three-way junctions. Although the structure of both types of three-way junctions is known, there have been no studies, especially on DNA intramolecular junctions, on the types of stacking involved in both

Submitted May 5, 2017, and accepted for publication June 14, 2017.
*Correspondence: lmarky@unmc.edu
Editor: Nadrian Seeman.
http://dx.doi.org/10.1016/j.bpj.2017.06.024

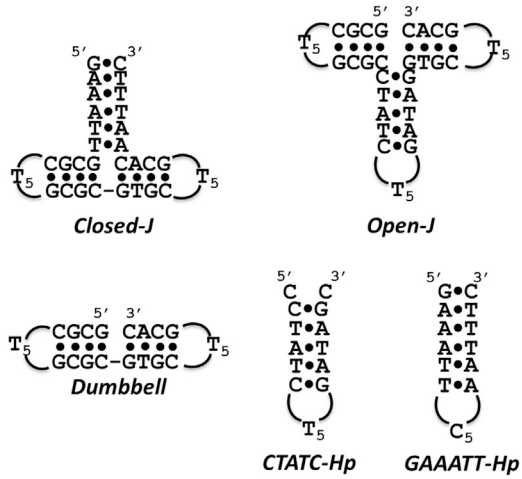

FIGURE 1 Cartoon of the sequences of DNA three-way junctions, drawn according to their hypothesized structure, with the *Dumbbell* forming the base of both three-way junctions upon which the different hairpins are stacked on top.

junctions and whether the state of the junction affects this stacking.

Current understanding of these junctions is based on the structure and stability of DNA and RNA obtained from previous thermodynamic investigations of their helix-coil transitions (23–27). Our laboratory is primarily focused on understanding the folding/unfolding of single-stranded DNA oligomers that are designed specifically to adopt intramolecular structures (28–30). Investigation of the physical properties of their 100% helical conformations over a wider temperature range yielded transition temperatures higher than their bimolecular counterparts due to a lower entropy penalty (28). Intramolecular structures are therefore amenable to detailed investigation into their thermodynamic parameters, allowing us to obtain additional parameters such as heat capacity.

In this work, we present a thermodynamic description of the unfolding of DNA intramolecular three-way junctions. Specifically, we used a combination of spectroscopic and calorimetric techniques to investigate the folding/unfolding thermodynamics of two three-way junctions with a closed or open junction and appropriate control stem-loop motifs. The overall results show that both junctions are stable over a wide range of salt concentrations. However, the open three-way junction is more stable due to a higher enthalpy contribution from the formation of a higher number of base-pair stacks.

MATERIALS AND METHODS

Materials

The oligonucleotides and their designations (Fig. 1) are as follows: d(5′-GAAATTC$_5$AATTTC-3′), *GAAATT-Hp;* d(5′-CCTATCT$_5$GATAGC-3′), *CTATC-Hp*; d(5′-GCGCT$_5$GCGCGTGCT$_5$GCAC-3′), *Dumbbell*; d(5′-GAAATTGCGCT$_5$GCGCGTGCT$_5$GCACAATTTC-3′), *Closed-J*; and d(5′-GCGCT$_5$GCGCCTATCT$_5$GATAGGTGCT$_5$GCAC-3′), *Open-J*. All DNA molecules were synthesized by IDT (Coralville, IA), reverse-phase HPLC purified, desalted on a G-10 Sephadex column, and lyophilized to dryness before use in experiments. The sequences of the three-way junctions, the control hairpins and dumbbell, and their hypothesized structures are shown in Fig. 1.

The concentration of each oligomer solution was determined from absorbance measurements at 260 nm at 90°C using the molar absorptivities, in mM^{-1} cm^{-1} of strands, reported as follows: 161.4 (*GAAATT-Hp*), 158.1 (*CTATC-Hp*), 222.9 (*Dumbbell*), 348.6 (*Closed-J*), and 364.5 (*Open-J*). These values were calculated by extrapolation of the tabulated values of the dimer and monomer bases from 25°C to high temperatures, using procedures reported earlier (31,32). Buffer solutions consisted of 10 mM sodium phosphate buffer and pH 7.0, adjusted with different salt concentrations up to 0.2 M NaCl. All chemicals used in this study were reagent grade and used without further purification.

Temperature-dependent UV spectroscopy, UV melting curves

Absorbance versus temperature profiles (i.e., UV melting curves) were measured at 268 nm with a thermoelectrically controlled 14 DS UV/Vis spectrophotometer (Aviv, Lakewood, NJ). The 268 nm was chosen because this wavelength follows the absorbance changes of both AT and GC base-pairs. The temperature was scanned from 1 to 100°C at a heating rate of ~0.6°C/min. Analysis of the shape of the melting curves yielded transition temperatures, T_M, which correspond to the inflection point of the helix-coil transitions and van 't Hoff enthalpies, ΔH_{vH}, using standard procedures (33). To determine the molecularity of the transition(s) of each DNA molecule, we investigated the dependence of T_M over at least a 10-fold range of total strand concentration. If the T_M remains constant in this range of strand concentration it indicates a monomolecular or intramolecular transition (33). Additional UV melting curves were obtained as a function of salt concentration to determine the differential binding of ions.

Circular dichroism spectroscopy

The conformation of each oligonucleotide was determined by simple inspection of the circular dichroism (CD) spectra at temperatures at which the structure of each oligonucleotide is 100% helical. These CD spectra were obtained from 320 to 220 nm in 1 nm increments, using a model No. 202SF CD spectrometer (Aviv) equipped with a Peltier temperature control system. The experimental CD melting curves were converted to α-curves with "α" being the fraction of strands in the helical state (33). Analysis of the CD melting curves yielded T_M values and ΔH_{vH} using procedures reported in Marky and Breslauer (33).

Differential scanning calorimetry

The total heat required for the unfolding of each oligonucleotide (hairpin, dumbbell, or three-way junction) was measured with a VP-DSC (differential scanning calorimeter, DSC) from Malvern MicroCal (Northampton, MA). These thermograms were obtained with a temperature ramp of ~0.75°C min^{-1} with oligomers ranging in concentration from 50 to 200 μM in total strands. Analysis of the thermograms yielded T_M values and standard thermodynamic profiles using the following relationships: (30,33) $\Delta H_{cal} = \int \Delta C_p(T)dT$ and $\Delta S_{cal} = \int \Delta C_p(T)/TdT$, and the Gibbs equation $\Delta G^\circ_{(T)} = \Delta H - T\Delta S$, where $\Delta C_p(T)$ is the anomalous heat capacity of the oligonucleotide solution during the unfolding process; ΔH_{cal} and ΔS_{cal} are the unfolding enthalpy and entropy, respectively, both assumed to be temperature-independent; and $\Delta G^\circ_{(T)}$ is the free energy at a temperature T. Alternatively, $\Delta G^\circ_{(T)}$ can be calculated using the equation

$\Delta G^{\circ}_{(T)} = \Delta H_{cal}(1 - T/T_M)$. Additional DSC experiments were obtained at several salt concentrations to indirectly obtain the associated heat capacity contributions, ΔC_p, which were determined from the slopes of the lines of the ΔH_{cal} versus T_M plots. The ΔH_{vH} terms were also obtained from the DSC thermograms and correspond to the unfolding of a cooperative unit, assuming a two-state transition. Simple inspection of the $\Delta H_{vH}/\Delta H_{cal}$ ratio provides information about the nature of the transition (33,34). A $\Delta H_{vH}/\Delta H_{cal}$ ratio of 0.9–1 indicates that all transitions are two-state (34) i.e., unfolding takes place without the presence of intermediates.

Determination of the differential binding of counterions

Additional UV melting curves were obtained as a function of salt concentration to determine the differential binding of counterions, Δn_{Na^+}. This Δn_{Na^+} linking number is measured experimentally using the following relationship (35–38):

$$\Delta n_{Na^+} = 1.11\left(\Delta H_{cal}/RT_M^2\right)\left[\partial T_M/\partial \ln\left[Na^+\right]\right]. \quad (1)$$

The $(\Delta H_{cal}/RT_M^2)$ term of Eq. 1 is determined directly from DSC experiments, whereas the term in brackets is determined from the slopes of the plots of T_M as a function of the concentration of salt, ranging from 16 to 216 mM. The 1.11 value in Eq. 1 is a constant, used to convert the activity of Na^+ into its concentration term i.e., $(Na^+) = 0.9[Na^+]$, where 0.9 is the activity coefficient over this range of salt concentration.

RESULTS

This work focuses on investigating the thermodynamic unfolding of two DNA three-way junctions containing either an open (*Open-J*) or closed (*Closed-J*) junction. We compare the unfolding of these two molecules with control molecules, consisting of a *Dumbbell*, which is identical for both three-way junctions and forms the base of both, as well as two hairpins that form the third stem of each three-way junction. UV melting curves were done to determine if the unfolding of each stem-loop motif takes place intramolecularly by testing the effect of strand concentration on the T_M, and to investigate their preliminary melting behavior. CD spectroscopy was used to determine the conformation of the three-way junctions and of the control molecules, and monitor the change in basepair stacking as a function of temperature. The unfolding thermodynamics of all molecules was investigated using DSC. The combined results from UV to DSC analysis were used to measure the differential binding of counterions during the folding and unfolding of these molecules. The thermodynamic parameters obtained from these experiments were compared to determine the effects of an open or closed junction on the unfolding of a three-way junction.

All molecules folded intramolecularly

Typical UV melting curves in 10 mM sodium phosphate (NaPi) buffer at pH 7.0 are shown in Fig. 2 (*left*). All the melting curves are sigmoidal and show cooperative unfolding of basepairs and basepair stacks. The T_M values for the transitions of each oligonucleotide remain constant across a

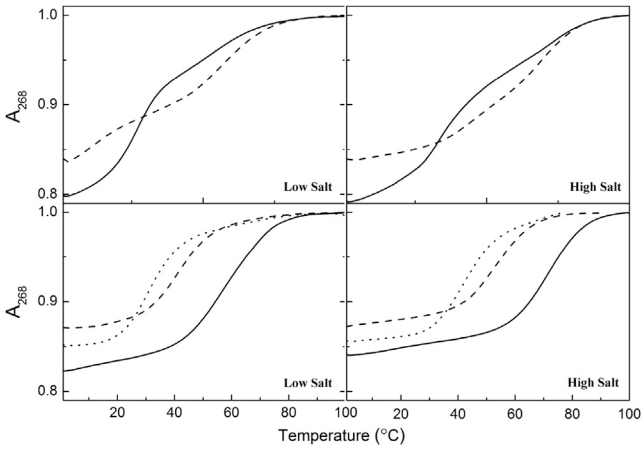

FIGURE 2 UV melting curves at 268 nm in 10 mM NaPi at pH 7.0 (*left panels*) and in 10 mM NaPi, 0.2 M NaCl at pH 7.0 (*right panels*); T_M (± 0.5°C) using oligonucleotide concentrations of 2 μM. (*Top panels*) Shown here are melting curves of *Closed-J* (*solid line*) and *Open-J* (*dashed line*). (*Bottom panels*) Shown here are melting curves of *Dumbbell* (*solid line*), *CTATC-Hp* (*dashed line*), and *GAAATT-Hp* (*dotted line*).

10-fold increase in strand concentration (Fig. S1), which is consistent with intramolecular unfolding.

The helix-coil transition of the hairpins and dumbbell take place as a monophasic transition with a hyperchromic effect regardless of salt concentration (*bottom panels* of Fig. 2; Fig. S2). Hyperchromicities are a measure of the strength of basepair stacking as well as number of basepair stacks, i.e., when comparing oligonucleotides with similar number of basepair stacks and stack composition, higher hyperchromicities indicates stronger basepair stacking (39,40). The hyperchromicities of the control molecules follow the order: 13% (*CTATC-Hp*) <15% (*GAAATT-Hp*) < and 18% (*Dumbbell*) at 268 nm. The melting curves for the hairpins and dumbbell have T_M values increasing from 30.9°C (*GAAATT-Hp*) <41.0°C (*CTATC-Hp*) <58.6°C (*Dumbbell*). Analysis of the UV-melting curves reveal that whereas the *CTATC-Hp* is more thermally stable, the hyperchromicities indicate that the *CTATC-Hp* has weaker basepair stacking, which follows the nearest-neighbor predictions of the enthalpy of CT/GA versus AA/TT basepair stacks. Analysis of the shape of the UV melting curves yielded average ΔH_{vH} values of 40 kcal/mol (*GAAATT-Hp*), 39 kcal/mol (*CTATC-Hp*), and 30 kcal/mol (*Dumbbell*). The ΔH_{vH}, or the folding enthalpy of the cooperative unit, for the *Dumbbell* is less than half of the predicted total enthalpy value, indicating that the two domains of *Dumbbell* melt simultaneously as a whole unit instead of two sequential transitions. At higher salt, all three parameters follow the same order at both salt concentrations.

Both three-way junctions unfold in a biphasic manner (*top* of Fig. 2; Fig. S2) with hyperchromicities of 20 (*Closed-J*) and 16% (*Open-J*) regardless of salt concentration. The lower hyperchromicity value of *Open-J* indicates weaker basepair stacking. Both three-way junctions have

similar overall structures but differ by their third stem sequence and in whether the junction is closed or open (Fig. 1). *Closed-J*, with a closed junction, has two transitions at 26.0 and 55.1°C with ΔH_{vH} values of 35 and 31 kcal/mol (Table 1) in low salt buffer. In high salt buffer containing 0.2 M NaCl, the T_M values of both transitions increase significantly (34.5 and 73.1°C) but the ΔH_{vH} values are only slightly higher (41 and 39 kcal/mol). *Open-J*, which has an open junction, has two transitions at 9.3 and 56.7°C with ΔH_{vH} values of 21 and 27 kcal/mol (Table 1). Upon increasing the salt concentration, the T_M values of both transitions increase (48.0 and 68.6°C) but the first transition increases by 38.7°C. Both ΔH_{vH} remain relatively unchanged (28 and 34 kcal/mol) even for the first transition with a large increase in thermal stability.

These junctions should have three stems of varying nucleic acid composition and sequence and therefore should have three different transitions. Their actual sequences may contribute to the inability to resolve three transitions. Although the *Dumbbell* should unfold biphasically, its UV melting curve (Fig. 2) shows only one transition, similar to the hairpins. Fig. 3 shows combined melting curves of the *Dumbbell* with the individual hairpins but there are only two resolved transitions for both three-way junctions regardless of salt concentration. The simultaneous unfolding of the *Dumbbell* alone and in both three-way junctions is reflected in the ΔH_{vH} values, which in total are much smaller than predicted (23,41), indicative of two stems melting simultaneously.

Closed-J retains the integrity of each stem better than *Open-J*

Fig. 3 (*top left*) shows the low salt UV melting curves of *Closed-J* compared to the combined melting curve of *Dumbbell* + *GAAATT-Hp*. Both curves have two transitions and different hyperchromicities, with the first transition T_M corresponding to that of the *GAAATT-Hp* and being unchanged in the curve of *Closed-J*. The T_M value of the second transition is ~4°C higher in the combined curve than the melt of *Closed-J*. However, the ΔH_{vH} values do not reflect this change (Table 1). A similar comparison at high salt concentration is shown in Fig. 3 (*top right*) and two transitions are still observed with higher T_M values and different hyperchromicities. Unlike the melting curves in low salt buffer, the T_M values of both transitions in *Closed-J* are similar to those in the combined melt.

Fig. 3 (*bottom left*) shows the UV melting curve of *Open-J* compared to the combined melting curve of *Dumbbell* + *CTATC-Hp* in low salt buffer. The combined melting curve consists of only one broad transition whereas the melting curve of *Open-J* displays two transitions. The first transition corresponds to the *CTATC-Hp* but with a much lower T_M. The second transition seen in the melt of *Open-J* overlays with that of the combined melt, which indicates that the open junction does not disrupt the structure of *Dumbbell* as is seen in *Closed-J*. At higher salt (Fig. 3, *bottom right*) the *CTATC-Hp* transition in *Open-J* is stabilized relative to the CTATC transition in the combined melting curve, indicating that high salt is stabilizing the stem, yielding a fully folded structure. The second transition corresponds to the *Dumbbell* structure in both melts with similar T_M values.

TABLE 1 T_M Values and ΔH_{vH} Obtained from UV and CD Melting Curves

	UV		CD	
Transition	T_M (°C)	ΔH_{vH} (kcal/mol)	T_M (°C)	ΔH_{vH} (kcal/mol)
		Closed-J		
First	26.0 (34.5)	35 (41)	29.0	34
Second	55.1 (73.1)	31 (39)	54.5	28
		Open-J		
First	9.3 (48.0)	21 (28)	—	—
Second	56.7 (68.6)	27 (34)	59.6	30
		Dumbbell		
	58.6 (71.8)	30 (39)	63.3	25
		GAAATT-Hp		
	30.9 (42.0)	40 (37)	30.5	37
		CTATC-Hp		
	41.0 (54.4)	39 (36)	39.8	25

All experiments were done in 10 mM NaPi buffer, at pH 7.0. Experimental errors are as follows: T_M (±0.5°C) and ΔH_{vH} (±15%). Values in parentheses correspond to experiments done in 10 mM NaPi buffer, 0.2 M NaCl at pH 7.0.

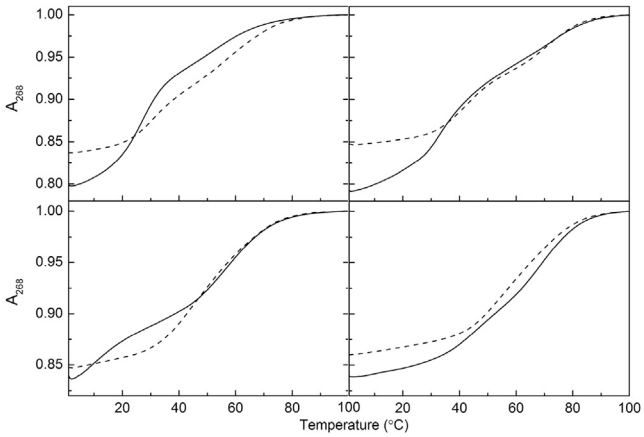

FIGURE 3 Combined UV melting curves at 268 nm in 10 mM NaPi at pH 7.0 (*left panels*) and in 10 mM NaPi, 0.2 M NaCl at pH 7.0 (*right panels*) are shown. (*Top panels*) Given here are melting curves of *Closed-J* (*solid line*) and *Dumbbell* + *GAAATT-Hp* (*dashed line*). (*Bottom panels*) Given here are melting curves of *Open-J* (*solid line*) and *Dumbbell* + *CTATC-Hp* (*dashed line*).

Closed-J has more basepair stacking contributions than *Open-J*

The left panels of Fig. 4 show the CD spectra of all molecules at 5°C. At this temperature, all oligonucleotides are

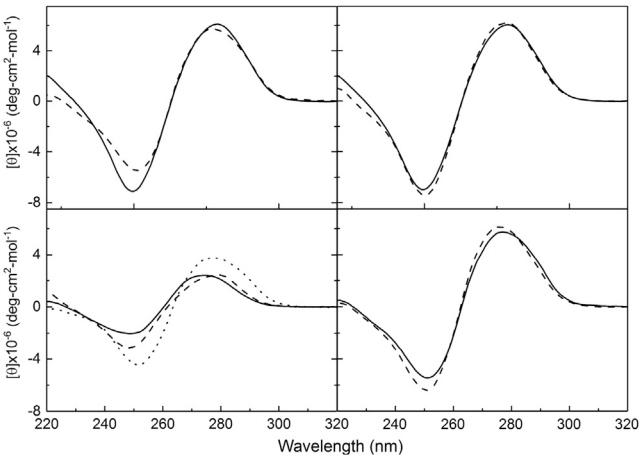

FIGURE 4 (*Left*) CD spectra at 5°C in 10 mM NaPi at pH 7.0. (*Top left*) CD spectra of *Closed-J* (*solid line*) and *Open-J* (*dashed line*) are given. (*Bottom left*) CD spectra of *Dumbbell* (*dotted line*), *CTATC-Hp* (*solid line*), and *GAAATT-Hp* (*dashed line*) are given. (*Top right*) CD spectra of *Closed-J* (*solid line*) and *Dumbbell* + *GAAATT-Hp* (*dashed line*) are given. (*Bottom right*) Shown here are CD spectra of *Open-J* (*solid line*) and *Dumbbell* + *CTATC-Hp* (*dashed line*).

fully folded and the spectra show a positive band centered at ~280 nm, related to the sugar puckering of the DNA, and a negative band at ~250 nm, corresponding to the extent of basepair stacking. The two bands are approximately equivalent in magnitude and indicate that all molecules are adopting a B-like conformation. The magnitude of the band at 250 nm can be viewed in a similar manner as hyperchromicity, with a weaker band indicating weaker basepair stacking. For instance, the magnitude of the peak at 250 nm of *CTATC-Hp* is reduced compared to *GAAATT-Hp*, which correlates well with the observed hyperchromicities of the UV melting curves. This indicates that *CTATC-Hp* is more thermally stable but has a lower number of basepair stacks than the *GAAATT-Hp*. In addition, the spectrum of *Open-J* as compared to that of *Closed-J* (Fig. 4, *top left*) shows a significant disparity at ~250 nm, indicating that there are fewer contributions from basepair stacking in *Open-J*.

Fig. 4 (*top right*) shows the CD spectrum of *Closed-J* compared with the combined spectrum of *Dumbbell* + *GAAATT-Hp* at low salt. The spectra are similar with a slight disparity at 250 nm, indicative of similar basepair stacking contributions. Fig. 4 (*bottom right*) shows the CD spectrum of *Open-J* compared to the combined CD spectrum of *Dumbbell* + *CTATC-Hp*. The spectra are similar but with a greater disparity at 250 nm, indicating a lower number of basepair stacking contributions in *Open-J*.

The CD melting curves of all molecules in 10 mM NaPi buffer at pH 7.0 are shown in Fig. S3 in terms of α as a function of temperature (33). Analysis of the *Closed-J* melting curve yielded two transitions with T_M values (29.0 and 54.5°C) and ΔH_{vH} values (34 and 28 kcal/mol), which were corroborated by the differentiated curve and are similar to those obtained from the UV melting curves (Table 1). The discrepancies in T_M values may be due to the ellipticity changes that measure basepair stacking alone. The T_M of the first transition is identical to that obtained for the *GAAATT-Hp* alone, but the T_M of the second transition is lower than that obtained for the *Dumbbell* alone. The CD melting curve of *Open-J* has only one observable transition (T_M of 59.6°C and ΔH_{vH} of 30 kcal/mol) corresponding to the unfolding of the *Dumbbell* structure. The T_M of this transition is closer to that of the *Dumbbell* alone than in *Closed-J*, indicating that whereas the open junction appears to destabilize the CTATC stem, it affects the *Dumbbell* less than a closed junction.

Calorimetric unfolding of an open and closed three-way junction as a function of salt concentration

DSC curves in low salt buffer and with additional salt concentrations are shown in Figs. 5 and 6 for each oligonucleotide and the resulting thermodynamic parameters are shown in Tables 2 and 3. The unfolding of each molecule undergoes highly reproducible monophasic or biphasic transitions. The T_M values obtained from the calorimetric melts, at higher strand concentrations, are similar to those obtained from UV melts, consistent with their intramolecular formation.

We obtained total unfolding enthalpies, ΔH_{cal}, of 117.1 kcal/mol (*Closed-J*) and 91.8 (*Open-J*) at low salt, and 118.8 kcal/mol (*Closed-J*) and 122.3 kcal/mol (*Open-J*) at 0.2 M NaCl concentration. These ΔH_{cal} values are in excellent agreement with the nearest neighbor enthalpies

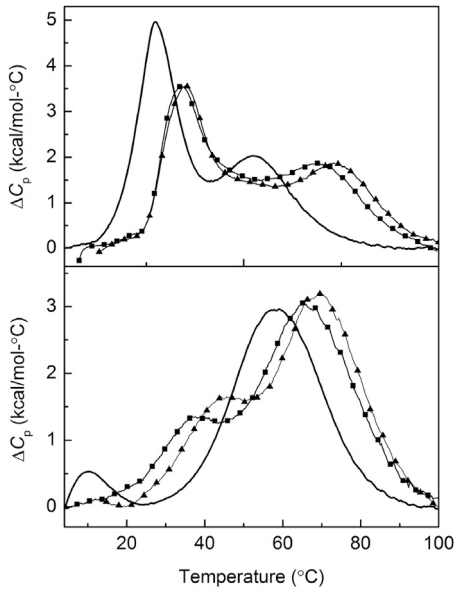

FIGURE 5 DSC curves of *Closed-J* (*top*) and *Open-J* (*bottom*) in 10 mM NaPi buffer at pH 7.0 (*solid lines*); with the addition of 0.1 M NaCl (*squares*); or with the addition of 0.2 M NaCl (*triangles*).

TABLE 2 Thermodynamic Profiles for the Folding of Intramolecular Hairpins and Junctions in 10 mM NaPi Buffer pH 7.0

	T_M (°C)	ΔH_{cal} (kcal/mol)	ΔH_{pred} (kcal/mol)	ΔC_p (cal/°C−mol)	ΔH_{vH} (kcal/mol)	$\Delta G^\circ_{(5)}$ (kcal/mol)	$T\Delta S_{cal}$ (kcal/mol)
				Closed-J			
First	27.8	−64.5	—	−730	−52	−4.9	59.6
Second	52.7	−52.6	—	440	−32	−7.7	44.9
Total		−117.1	−117.5	−290	—	−12.6	104.5
				Open-J			
First	10.9	−5.7	—	−840	−61	−0.1	−5.6
Second	59.0	−86.1	—	−280	−31	−14.0	−72.1
Total		−91.8	−116.0	−1120	—	−14.1	−77.7
				Dumbbell			
First	54.8	−43.4	—	—	−39	−6.6	−36.8
Second	68.0	−34.0	—	—	−45	−6.3	−27.7
Total		−77.4	−75.8	600	−84	−12.9	−64.5
				CTATC-Hp			
	41.3	−43.8	−37.8	330	−35	−5.1	−38.7
				GAAATT-Hp			
	29.7	−44.0	−39.1	140	−42	−3.6	−40.4

Experimental errors are as follows: T_M (±0.5°C), ΔH_{cal} (±5%), ΔC_p (±20%), ΔH_{vH} (±15%), $T\Delta S_{cal}$ (±5%), $\Delta G^\circ_{(5)}$ (±7%).

of 117.5 kcal/mol (*Closed-J*) and 116.0 kcal/mol (*Open-J*), estimated in 1 M NaCl concentrations (25) by considering all the potential basepair stacks for the three-way junctions shown in Fig. 1. The ΔH_{cal} of the control molecules are as follows in low/high salt: 43.8/40.9 kcal/mol (*CTATC-Hp*), 44.0/41.0 kcal/mol (*GAAATT-Hp*), and 77.4/71.9 kcal/mol (*Dumbbell*); also in excellent agreement with the nearest neighbor parameters (25). In addition, these control molecules yielded negligible positive folding heat capacity effects, 140 cal/mol-K (*GAAATT-Hp*) to 600 cal/mol-K (*Dumbbell*), which are contrary to the negative heat capacity effects of the junctions.

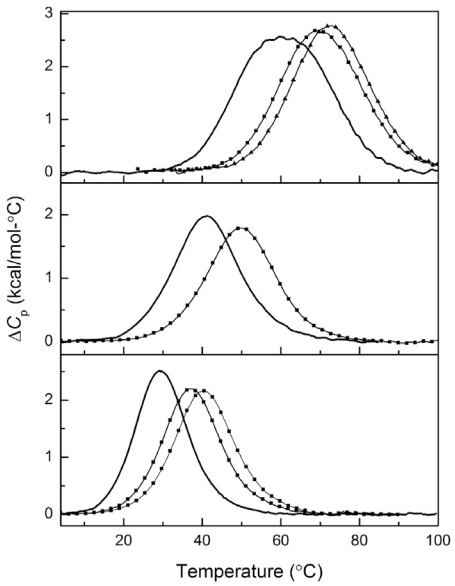

FIGURE 6 DSC curves are shown of *Dumbbell* (*top*), *CTATC-Hp* (*middle*), and *GAAATT-Hp* (*bottom*) in 10 mM NaPi buffer at pH 7.0 (*solid lines*); with the addition of 0.1 M NaCl (*squares*); or with the addition of 0.2 M NaCl (*triangles*).

The DSC thermogram of *Closed-J* in low salt unfolds biphasically, with the first transition roughly corresponding to the unfolding of the GAAATT stem and the second transition corresponding to the unfolding of the GCGC stem. The actual ΔH_{cal} values of these transitions (Table 2) indicate that the GTGC stem is melting within both transitions. Upon increasing the salt concentration to 0.1 M NaCl, both transitions are shifted to higher temperatures and a third transition becomes visible. All three transitions are further resolved upon increasing the salt concentration to 0.2 M NaCl. The ΔH_{cal} for each of these three transitions corresponds roughly with the predicted enthalpies of the individual stems (Table 3), indicating disruption of their simultaneously unfolding. In addition, both transitions in low salt yielded $\Delta H_{vH}/\Delta H_{cal}$ ratios of <0.9, whereas at high salt the ratios become ~1 for each of the three transitions, indicating each stem unfolds in a two-state manner. We obtained a negligible heat capacity effect (ΔC_p = 290 cal/mol-K) for the folding of *Closed-J*, i.e., the folded and unfolded states have a similar exposure of hydrophobic/hydrophilic groups to the solvent.

The DSC of *Open-J* in low salt unfolds biphasically with the first transition corresponding to the unfolding of the CTATC stem whereas the second transition corresponds to the unfolding of the *Dumbbell*. The small ΔH_{cal} value (5.6 kcal/mol) for the first transition is equivalent to the melting of one basepair stack in the CTATC stem. Both transitions shift to higher temperatures upon increasing the salt concentration to 0.2 M NaCl. The ΔH_{cal} of the second transition is only slightly larger, but the ΔH_{cal} of the first transition increases by ~27.4 kcal/mol, which indicates the full formation of the CTATC stem. We obtained a small heat capacity effect (ΔC_p = −1120 cal/mol-K), which indicates the unfolded state of *Open-J* is exposing a slightly larger number of hydrophilic groups to the solvent than the random coil state. Furthermore, $\Delta H_{vH}/\Delta H_{cal}$ ratios of

TABLE 3 Thermodynamic Profiles for the Folding of Intramolecular Hairpins and Junctions in 10 mM NaPi, 0.2 M NaCl pH 7.0

	T_M (°C)	ΔH_{cal} (kcal/mol)	ΔH_{vH} (kcal/mol)	$\Delta G^\circ_{(5)}$ (kcal/mol)	$T\Delta S_{cal}$ (kcal/mol)	Δn_{ion}
			Closed-J			
First	35.6	−41.5	−58	−4.1	−37.4	−0.97
Second	50.6	−34.8	−30	−4.9	−29.9	
Third	74.6	−42.8	−38	−8.5	−34.0	−186
Total		−118.8		−17.5	−101.3	−2.83 (−0.098)
			Open-J			
First	43.8	−33.1	−32.9	−3.0	−30.1	−2.46
Second	70.4	−89.2	−33.8	−17.0	−72.2	−2.01
Total		−122.3		−20.0	−102.3	−4.47 (−0.160)
			Dumbbell			
Total	72.9	−71.9	−37	−14.1	−57.8	02.03 (−0.127)
			CTATC-Hp			
	50.0	−40.9	−36.3	−5.7	−35.2	−1.02 (−0.085)
			GAAATT-Hp			
	40.6	−41.0	−39.8	−4.7	−36.3	−1.06 (−0.088)

Experimental errors are as follows: T_M (±0.5°C), ΔH_{cal} (±5%), ΔH_{vH} (±15%), $T\Delta S_{cal}$ (±5%), $\Delta G^\circ_{(5)}$ (±7%), and $\Delta n_{Na}+$ (±12%).

10.7 and 0.36 are obtained for the first and second transition of *Open-J*, respectively. The value of 10.7 is unrealistic, due to the absence of a good pretransition baseline because of its low T_M. The small value of the second transition indicates two stems (i.e., *Dumbbell*) are melting simultaneously. At higher salt, the ratio for the first transition becomes 1, indicating a two-state transition whereas the $\Delta H_{vH}/\Delta H_{cal}$ ratio of the second transition remains unchanged.

A closed junction disrupts the cooperative unfolding of the junction

Fig. 7 (*top left*) shows the DSC thermogram of *Closed-J* compared to the combined thermogram of *Dumbbell* + *GAAATT-Hp* in low salt buffer. The total experimental enthalpy of *Closed-J* (117.1 kcal/mol) closely matches the enthalpy of the combined thermogram (121.4 kcal/mol).

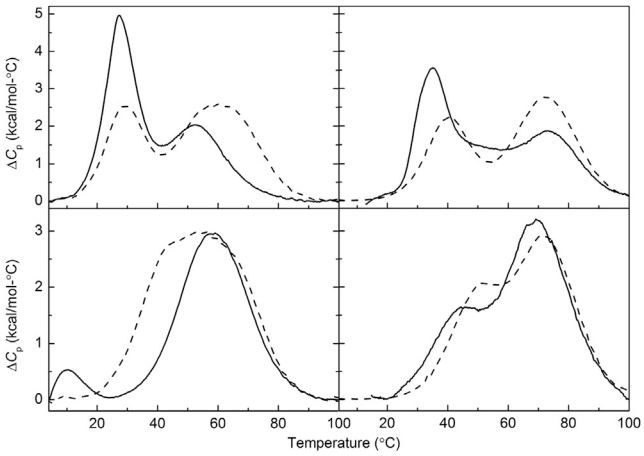

FIGURE 7 Combined DSC thermograms in (*left*) 10 mM NaPi at pH 7.0 and (*right*) 10 mM NaPi, 0.2 M NaCl, pH 7.0; T_M (±0.5°C). (*Top*) Given here are combined DSC thermogram of *Closed-J* (*solid line*); *Dumbbell* + *GAAATT-Hp* (*dotted line*). (*Bottom*) Shown here is a DSC thermogram of *Open-J* (*solid line*), *Dumbbell* + *CTATC-Hp* (*dotted line*).

The T_M of the first transition in both curves overlap and corresponds to the unfolding of the GAAATT stem. However, the enthalpy of the first transition in *Closed-J* is much greater than *GAAATT-Hp* alone (Table 2) and suggests at least part of the GTGC stem is unfolding simultaneously, disrupting the cooperative unfolding of the dumbbell structure. The second transition corresponds in both curves to an unfolding event that includes the GCGC stem but with a lower enthalpy and T_M (~8.7°C compared to the average T_M value of *Dumbbell*) in *Closed-J* compared to the combined curve.

Fig. 7 (*top right*) shows the DSC thermogram of *Closed-J* compared to the combined thermogram of *Dumbbell* + *GAAATT-Hp* in high salt buffer. The overall enthalpies are in excellent agreement, 118.8 and 122.9 kcal/mol, respectively. The combined thermogram yields two distinct transitions corresponding to the GAAATT stem and *Dumbbell* whereas *Closed-J* unfolds in three transitions corresponding to its three individual stems. The third transition occurs in the 45–60°C temperature range and is obviously present during deconvolution of the data, as omitting this transition leaves a significant amount of heat capacity unaccounted for.

An open junction retains the integrity and cooperative unfolding of the junction

Fig. 7 (*bottom left*) shows the DSC thermogram of *Open-J* compared to the combined thermogram of *Dumbbell* + *CTATC-Hp* in low salt. The total experimental enthalpy of *Open-J* (91.8 kcal/mol) is lower than the enthalpy of the combined thermogram (121.2 kcal/mol) by 29.4 kcal/mol. In the combined curve, the peak associated with the unfolding of the CTATC stem occurs at ~42°C and is absent in the thermogram of *Open-J* or rather, it occurs at 10°C, a 32°C difference. In both curves, the second transition corresponds to the unfolding of the *Dumbbell* structure and has nearly identical T_M values and enthalpies.

Fig. 7 (*bottom right*) shows the DSC thermogram of *Open-J* compared to the combined thermogram of *Dumbbell* + *CTATC-Hp* in high salt. The total experimental enthalpy of *Open-J* (122.3 kcal/mol) closely matches the enthalpy of the combined thermogram (112.8 kcal/mol). Both curves show two distinct transitions corresponding to the CTATC stem and the *Dumbbell* structure. The CTATC transition occurs ~6°C lower than in the combined thermogram with an enthalpy matching what was obtained for the control hairpin. This signifies that all three stems are stabilized and fully formed.

Open-J has a higher uptake of counterions than *Closed-J*

We used Eq. 1 to calculate the differential binding of counterions (Table 3). The slope of the T_M dependences on salt concentration is obtained from UV melting curves as a function of salt concentration (Fig. S4) and the average $\Delta H_{cal}/RT_M^2$ term is obtained from the DSC melts at several salt concentrations. The folding of each molecule is accompanied by an uptake of ions, due to the shift of the helix-coil equilibrium toward the conformation with a higher charge density parameter (42). The $\Delta n_{Na}{}^+$ values are presented in the last column of Table 3 and their magnitude indicates the strength of ion binding by the helical stem of each molecule. We obtained $\Delta n_{Na}{}^+$s of −0.97 and −1.86 mol Na^+/mol molecule (first and second transition, respectively) for *Closed-J* and −2.46 and −2.01 mol Na^+/mol molecule (first and second transition, respectively) for *Open-J*. These values can be normalized per helical phosphate by considering the total number of helical phosphates, including the two loop phosphates adjacent to each stem, yielding a total of 29 helical phosphates for *Closed-J* and 28 for *Open-J*. This exercise yielded $\Delta n_{Na}{}^+$ values of 0.098 mol Na^+/mol phosphate for *Closed-J* and 0.160 mol Na^+/mol phosphate for *Open-J*; both values are lower than the 0.17 mol Na^+/mol phosphate value for long DNA duplexes (43–45). The $\Delta n_{Na}{}^+$ value of *Closed-J* is approximately equal to the additive $\Delta n_{Na}{}^+$ values of *Dumbbell* and *GAAATT-Hp*, and is consistent with the simultaneous folding of one to two of these stem domains (4–6 basepairs each) (46,47); (Table 2). The $\Delta n_{Na}{}^+$ value of *Open-J* is significantly higher (~1 additional stem higher) than the additive values of the *Dumbbell* and the *CTATC-Hp*; the first transition has a high contribution to the $\Delta n_{Na}{}^+$ value due to its high T_M dependence on salt, and this is because, at low salt, this stem is not completely formed, as discussed earlier. This long-range effect is consistent with the short-range effect of the enthalpy as a function of salt concentration.

The folding of *Open-J* is thermodynamically more favorable than Closed-J

Thermodynamic profiles for all transitions observed in the folding of each molecule are listed in Tables 2 and 3. In terms of the overall free energy contribution at 5°C, $\Delta G^\circ_{(5)}$, we obtained favorable $\Delta G^\circ_{(5)}$ terms at all salt concentrations. Notably, both junctions fold at low salt concentrations and this is because of the lower entropic penalty in the folding of intramolecular structures. Each transition has a favorable free energy term resulting from the characteristic compensation of a favorable enthalpy contribution with an unfavorable entropy contribution. Favorable heat contributions involve the formation of basepairs and basepair stacks, whereas unfavorable entropy contributions involve the ordering of the strands and ion and water binding. The enthalpy contributions were discussed in the previous sections. The entropy contributions, in energy terms ($T\Delta S_{cal}$), for the folding of each hairpin are shown in Tables 2 and 3. The magnitude of the unfavorable entropies follows the same order as those of the enthalpies.

In terms of the total folding free energy, *Open-J* is thermodynamically more favorable than *Closed-J* in low salt even though the first transition has a favorable $\Delta G^\circ_{(5)}$ of 0.1 kcal/mol, indicating that formation of this stem is not favorable. *Open-J* is enthalpically less favorable than *Closed-J* in low salt buffer, but it also has a more favorable entropy term. This, coupled with the increased thermal and enthalpic stability of the *Dumbbell* structure relative to *Closed-J*, leads to a higher overall $\Delta G^\circ_{(5)}$ of ~1.5 kcal/mol.

The increasing salt yielded an even more favorable $\Delta G^\circ_{(5)}$ term for *Open-J* over Closed-J by 2.5 kcal/mol. At higher salt, *Closed-J* is thermally more stable but gains little in the way of favorable enthalpy contributions. On the other hand, *Open-J* at higher salt has a large increase in thermal stability (~32.9°C) of the CTATC stem in addition to an increase in enthalpy of ~27.4 kcal/mol. This is coupled with a lower unfavorable entropy term leading to the large free energy term of the second transition of *Open-J* value, which is responsible for the ~2.5 kcal/mol difference between the two three-way junctions.

DISCUSSION

A closed junction is fully formed at low salt but disrupts base stacking around the junction, whereas an open junction is unstable at low salt, but does not disrupt base stacking at the junction

The main observation obtained from UV melting curves is that the closed junction disrupts basepair stacking around the junction of *Closed-J*, whereas the stem remains stable. Despite this instability, the results obtained from the UV melting curves indicate that at low salt, *Closed-J* is fully formed and can be accurately described by what is hypothesized in Fig. 1. This is not the case for *Open-J*, in which a decrease in thermal stability is caused by the open junction, which affects the basepairs stacking of the CTATC stem-loop. The UV results for *Open-J* indicate that its structure cannot be accurately described by the structure in Fig. 1.

Both three-way junctions are stabilized by an increased salt concentration. These results are corroborated by analysis of the CD spectra, in which there is almost no disparity at 250 nm between *Closed-J* and its constituent molecules, whereas *Open-J* has a much larger difference that indicates fewer base-stacking contributions. Based on the UV and CD melts, the lack of base-stacking is related to the unstable CTATC stem, which is only partially formed in the UV melting curves and is not present at all in the CD melting curves.

A closed junction breaks up the cooperative unfolding of the dumbbell at higher salt, whereas an open junction retains the integrity of the junction

DSC analysis of *Closed-J* reveals that at low salt, the junction behaves similar to what is seen in the UV. However, analysis of the enthalpies reveals that the two transitions are made up of ~1.5 stems, with the first transition corresponding to the unfolding of the GAAATT stem and the second transition corresponding to the unfolding of the GCGC stem. The GTGC most likely begins melting with the GAAATT stem and finishes melting with the GCGC stem, indicating that even at low salt the dumbbell base is disrupted. However, the thermal instabilities seen for the unfolding of GTGC and GCGC stems compared to their control molecules do not correspond to a reduction in the enthalpy. At high salt, all three transitions are separated such that the unfolding of the GTGC stem is visible as a separate transition and all three transitions have an enthalpy corresponding almost exactly to the predicted enthalpies of the control stems. Thus, at high salt, *Closed-J* behaves as three separate noncooperative arms, which matches the results obtained from Δn_{ion} that *Closed-J* can be accurately described by the sum of the three stem-loop motifs. Or rather, the closed junction causes the overall structure to unfold in separate melting domains that decrease the T_M without compromising basepair stacking contributions (Fig. 8, *left cartoon*).

DSC analysis for the unfolding of *Open-J* confirms what is seen in UV at low salt, that the CTATC stem is almost completely unfolded whereas the dumbbell base is unaffected both thermally and enthalpically. The enthalpy of the first transition suggests that most of the CTATC is unfolded, presumably in the center where the weaker AT base-stacks are present (Fig. 8, *right cartoon*). The ΔH_{cal} of the second transition is higher than that of *Dumbbell* alone by 11.8 kcal/mol and the excess corresponds roughly to one GC/GC basepair stack. Upon increasing the salt concentration, the first transition gains a substantial increase in both thermal and enthalpic stability and matches the DSC of its component molecules. This result suggests that at physiological salt concentration, not only would an open junction be fully folded, but would also fold into a structure similar to what is hypothesized in Fig. 1.

Open-J is thermodynamically more favorable than *Closed-J* at all salt concentrations. At low salt, this is primarily due to the thermal and enthalpic stability of the dumbbell structure of *Open-J*, which gives this transition a folding free energy significantly higher than the comparable transition in *Closed-J*. At higher salt, *Closed-J* does not regain the stability of the dumbbell and thus the folding of its stems have not only a lower thermal stability but also a lower enthalpy, leading to a lower free energy. *Open-J* not only maintains the integrity of the dumbbell structure but regains the full folding of the CTATC stem, leading to its larger free energy term at high salt.

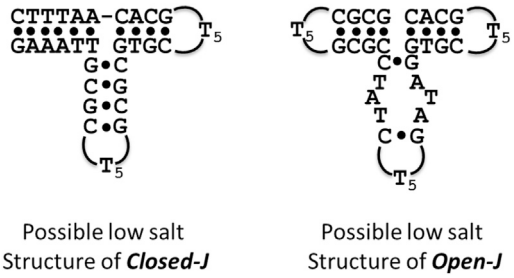

FIGURE 8 Cartoon of potential alternate structures of *Closed-J* and *Open-J*.

CONCLUSIONS

We have described the melting behavior of two intramolecular three-way junctions, which contain either an open or closed junction. The closed junction of *Closed-J* has a defined structure and retains the basepair stacking of all three stems. However, its junction sacrifices thermal stability of the *Dumbbell* structure to maintain an overall folded state. Although the overall shape and fold of the junction may be similar to what is shown in Fig. 1, DSC analysis indicates it may actually consist of the GAAATT stem stacked on the GTGC stem (Fig. 8, *left cartoon*). At higher salt concentrations, the simultaneous unfolding of the above domains is lost, resulting in unfolding of the three separate stems. In contrast, the open junction of *Open-J* in low salt maintains the thermal and enthalpic stability of the *Dumbbell* structure although sacrificing stability of the CTATC stem. The stability of the *Dumbbell* structure is a primary reason for the higher $\Delta G^{\circ}_{(5)}$ value seen for *Open-J* at low salt. Higher salt not only maintains thermal stability of the *Dumbbell* structure in *Open-J* but causes the CTATC stem to fully fold. In short, intramolecular DNA junctions, open or closed, can form even at low salt concentrations, maintaining its overall basepair stacking contribution, i.e., DNA junctions are flexible molecules. Future studies investigate how the inclusion of bulges at the junction sites affects their degree of flexibility and the inclusion of fluorescent bases will be used to examine the size of the cooperative units in these junctions.

SUPPORTING MATERIAL

Five figures are available at http://www.biophysj.org/biophysj/supplemental/S0006-3495(17)30674-4.

AUTHOR CONTRIBUTIONS

L.A.M. designed the experiments and assisted in writing the main article. C.E.C. performed the experiments and wrote the main article.

ACKNOWLEDGMENTS

This work was supported by grant MCB-1122029 from the National Science Foundation.

REFERENCES

1. de la Peña, M., D. Dufour, and J. Gallego. 2009. Three-way RNA junctions with remote tertiary contacts: a recurrent and highly versatile fold. *RNA.* 15:1949–1964.
2. Bikard, D., C. Loot, …, D. Mazel. 2010. Folded DNA in action: hairpin formation and biological functions in prokaryotes. *Microbiol. Mol. Biol. Rev.* 74:570–588.
3. Batey, R. T., S. D. Gilbert, and R. K. Montange. 2004. Structure of a natural guanine-responsive riboswitch complexed with the metabolite hypoxanthine. *Nature.* 432:411–415.
4. Buck, J., B. Fürtig, …, H. Schwalbe. 2007. Time-resolved NMR methods resolving ligand-induced RNA folding at atomic resolution. *Proc. Natl. Acad. Sci. USA.* 104:15699–15704.
5. Chi, Y. I., M. Martick, …, S. H. Kim. 2008. Capturing hammerhead ribozyme structures in action by modulating general base catalysis. *PLoS Biol.* 6:e234.
6. Dufour, D., M. de la Peña, …, J. Gallego. 2009. Structure-function analysis of the ribozymes of chrysanthemum chlorotic mottle viroid: a loop-loop interaction motif conserved in most natural hammerheads. *Nucleic Acids Res.* 37:368–381.
7. Kazantsev, A. V., and N. R. Pace. 2006. Bacterial RNase P: a new view of an ancient enzyme. *Nat. Rev. Microbiol.* 4:729–740.
8. Conn, G. L., D. E. Draper, …, A. G. Gittis. 1999. Crystal structure of a conserved ribosomal protein-RNA complex. *Science.* 284:1171–1174.
9. Klein, D. J., P. B. Moore, and T. A. Steitz. 2004. The roles of ribosomal proteins in the structure assembly, and evolution of the large ribosomal subunit. *J. Mol. Biol.* 340:141–177.
10. Bhuiyan, S. H., K. Gowda, …, C. Zwieb. 2000. Assembly of archaeal signal recognition particle from recombinant components. *Nucleic Acids Res.* 28:1365–1373.
11. Egea, P. F., R. M. Stroud, and P. Walter. 2005. Targeting proteins to membranes: structure of the signal recognition particle. *Curr. Opin. Struct. Biol.* 15:213–220.
12. Hainzl, T., S. Huang, and A. E. Sauer-Eriksson. 2002. Structure of the SRP19 RNA complex and implications for signal recognition particle assembly. *Nature.* 417:767–771.
13. Sauer-Eriksson, A. E., and T. Hainzl. 2003. S-domain assembly of the signal recognition particle. *Curr. Opin. Struct. Biol.* 13:64–70.
14. Chandler, M., F. de la Cruz, …, B. Ton-Hoang. 2013. Breaking and joining single-stranded DNA: the HUH endonuclease superfamily. *Nat. Rev. Microbiol.* 11:525–538.
15. Khan, S. A. 2005. Plasmid rolling-circle replication: highlights of two decades of research. *Plasmid.* 53:126–136.
16. Song, S. I., and W. A. Miller. 2004. *Cis* and *trans* requirements for rolling circle replication of a satellite RNA. *J. Virol.* 78:3072–3082.
17. Bouvier, M., M. Ducos-Galand, …, D. Mazel. 2009. Structural features of single-stranded integron cassette attC sites and their role in strand selection. *PLoS Genet.* 5:e1000632.
18. Mazel, D. 2006. Integrons: agents of bacterial evolution. *Nat. Rev. Microbiol.* 4:608–620.
19. Das, B., J. Bischerour, …, F. X. Barre. 2010. Molecular keys of the tropism of integration of the cholera toxin phage. *Proc. Natl. Acad. Sci. USA.* 107:4377–4382.
20. Val, M. E., M. Bouvier, …, F. X. Barre. 2005. The single-stranded genome of phage CTX is the form used for integration into the genome of *Vibrio cholerae*. *Mol. Cell.* 19:559–566.
21. Neelsen, K. J., and M. Lopes. 2015. Replication fork reversal in eukaryotes: from dead end to dynamic response. *Nat. Rev. Mol. Cell Biol.* 16:207–220.
22. Singleton, M. R., S. Scaife, and D. B. Wigley. 2001. Structural analysis of DNA replication fork reversal by RecG. *Cell.* 107:79–89.
23. Breslauer, K. J., R. Frank, …, L. A. Marky. 1986. Predicting DNA duplex stability from the base sequence. *Proc. Natl. Acad. Sci.* 83:3746–3750.
24. Rentzeperis, D. S., R. Maiti, …, L. A. Marky. 2002. Folding of intramolecular DNA hairpin loops: enthalpy-entropy compensations and hydration contributions. *J. Phys Chem.* 106:9945–9950.
25. SantaLucia, J., Jr., H. T. Allawi, and P. A. Seneviratne. 1996. Improved nearest-neighbor parameters for predicting DNA duplex stability. *Biochemistry.* 35:3555–3562.
26. Sugimoto, N., S. Nakano, …, M. Sasaki. 1995. Thermodynamic parameters to predict stability of RNA/DNA hybrid duplexes. *Biochemistry.* 34:11211–11216.
27. Xia, T., J. SantaLucia, Jr., …, D. H. Turner. 1998. Thermodynamic parameters for an expanded nearest-neighbor model for formation of RNA duplexes with Watson-Crick base pairs. *Biochemistry.* 37:14719–14735.
28. Lee, H. T., C. Carr, …, L. A. Marky. 2011. A thermodynamic approach for the targeting of nucleic acid structures using their complementary single strands. *Methods Enzymol.* 492:1–26.
29. Lee, H. T., C. M. Olsen, …, L. A. Marky. 2008. Thermodynamic contributions of the reactions of DNA intramolecular structures with their complementary strands. *Biochimie.* 90:1052–1063.
30. Marky, L. A., S. Maiti, …, I. Khutsishvili. 2007. Building blocks of nucleic acid nanostructures: unfolding thermodynamics of intramolecular DNA complexes. *In* Biomedical Applications of Nanotechnology. V. Labhasetwar and D. L. Leslie-Pelecky, editors. John Wiley & Sons, Hoboken, NJ, pp. 191–226.
31. Cantor, C. R., M. M. Warshaw, and H. Shapiro. 1970. Oligonucleotide interactions. 3. Circular dichroism studies of the conformation of deoxyoligonucleotides. *Biopolymers.* 9:1059–1077.
32. Borer, P. N. 1975. Optical properties of nucleic acids, absorptions and circular dichroism spectra. *In* Handbook of Biochemistry and Molecular Biology. G. D. Fasman, editor. CRC Press, Cleveland, OH, pp. 589–595.
33. Marky, L. A., and K. J. Breslauer. 1987. Calculating thermodynamic data for transitions of any molecularity from equilibrium melting curves. *Biopolymers.* 26:1601–1620.
34. Privalov, P. L., and S. A. Potekhin. 1986. Scanning microcalorimetry in studying temperature-induced changes in proteins. *Methods Enzymol.* 131:4–51.
35. Kaushik, M., N. Suehl, and L. A. Marky. 2007. Calorimetric unfolding of the bimolecular and I-motif complexes of the human telomere complementary strand, d(C(3)TA(2))(4). *Biophys. Chem.* 126:154–164.
36. Khutsishvili, I., S. Johnson, …, L. A. Marky. 2009. Unfolding thermodynamics of DNA intramolecular complexes involving joined triple- and double-helical motifs. *Methods Enzymol.* 466:477–502.
37. Khutsishvili, I., N. Zhang, …, V. Shafirovich. 2013. Thermodynamic profiles and nuclear magnetic resonance studies of oligonucleotide duplexes containing single diastereomeric spiroiminodihydantoin lesions. *Biochemistry.* 52:1354–1363.

38. Lee, H. T., I. Khutsishvili, and L. A. Marky. 2010. DNA complexes containing joined triplex and duplex motifs: melting behavior of intramolecular and bimolecular complexes with similar sequences. *J. Phys. Chem. B.* 114:541–548.

39. Freifelder, D., and P. F. Davison. 1962. Hyperchromicity and strand separation in bacterial DNA. *Biophys. J.* 2:249–256.

40. Thomas, R. 1993. The denaturation of DNA. *Gene.* 135:77–79.

41. SantaLucia, J., Jr. 1998. A unified view of polymer, dumbbell, and oligonucleotide DNA nearest-neighbor thermodynamics. *Proc. Natl. Acad. Sci. USA.* 95:1460–1465.

42. Nakano, S., M. Fujimoto, …, N. Sugimoto. 1999. Nucleic acid duplex stability: influence of base composition on cation effects. *Nucleic Acids Res.* 27:2957–2965.

43. Record, M. T., Jr., C. F. Anderson, and T. M. Lohman. 1978. Thermodynamic analysis of ion effects on the binding and conformational equilibria of proteins and nucleic acids: the roles of ion association or release, screening, and ion effects on water activity. *Q. Rev. Biophys.* 11:103–178.

44. Manning, G. S. 1978. The molecular theory of polyelectrolyte solutions with applications to the electrostatic properties of polynucleotides. *Q. Rev. Biophys.* 11:179–246.

45. Rentzeperis, D., K. Rippe, …, L. A. Marky. 1992. Calorimetric characterization of parallel-stranded DNA stability, conformational flexibility, and ion binding. *J. Am. Chem. Soc.* 114:5926–5928.

46. Rentzeperis, D., K. Alessi, and L. A. Marky. 1993. Thermodynamics of DNA hairpins: contribution of loop size to hairpin stability and ethidium binding. *Nucleic Acids Res.* 21:2683–2689.

47. Rentzeperis, D., D. P. Kharakoz, and L. A. Marky. 1991. Coupling of sequential transitions in a DNA double hairpin: energetics, ion binding, and hydration. *Biochemistry.* 30:6276–6283.